
Article:
Herod, Jordan D., Cowling, Stephen J. orcid.org/0000-0002-4771-9886 and Bruce, Duncan W. orcid.org/0000-0002-1365-2222 (2022) Synthesis and mesomorphism of 3,4-dialkoxyphenylpyridine complexes of silver(I). JOURNAL OF MOLECULAR LIQUIDS. 119707. ISSN 0167-7322

https://doi.org/10.1016/j.molliq.2022.119707

Journal of Molecular Liquids 362 (2022) 119707

Contents lists available at ScienceDirect

Journal of Molecular Liquids

journal homepage: www.elsevier.com/locate/molliq

Synthesis and mesomorphism of 3,4-dialkoxyphenylpyridine complexes of silver(I)

Jordan D. Herod, Stephen J. Cowling, Duncan W. Bruce *

Department of Chemistry, University of York, Heslington, York YO10 5DD, UK

ARTICLE INFO

Article history:
Received 3 May 2022
Revised 17 June 2022
Accepted 22 June 2022
Available online 24 June 2022

Keywords:
Metallomesogen
Silver
Phenylpyridine
Polycatenar

ABSTRACT

3,4-Dialkoxyphenylpyridine complexes with silver dodecyl sulfate or silver triflate are liquid crystalline. The complexes are polycatenar and show one or both of a cubic and a columnar hexagonal phase depending on the chain length of the dialkoxyphenylpyridine and the anion associated with the silver. Their mesomorphism is compared both with the analogous and very well-studied silver complexes of dialkoxystilbazole ligands as well as closely related *N*-phenylpyridinium analogues. The slightly shorter nature of the dialkoxyphenylpyridines is important in determining the mesomorphism when compared to the dialkoxystilbazole complexes, whereas there are appreciable differences with the *N*-phenylpyridinium salts. The notable stabilisation of the Col_h phase remains a feature of all three families of materials.

1. Introduction

Over several years, silver(I) complexes of mono-, di- and trialkoxystilbazoles (Fig. 1) have been prepared and used to elucidate many structure/property relationships relating to, for example, the formation of cubic phases – and also to phase transitions in polycatenar mesogens [1]. The stilbazoles have also proved valuable components of other mesomorphic metal complexes [2] as well as forming the acceptor unit for both hydrogen- and halogen-bonded liquid crystals [3].

Recently, there has been interest in related alkoxyphenylpyridines (Fig. 1). The 4-alkoxy derivatives have been used as halogen-bond acceptors in the formation of liquid-crystalline complexes of iodine and interhalogens [4], while the 3,4-dialkoxy derivatives have been used as intermediates in the preparation of polycatenar *N*-phenylpyridinium liquid crystals [5–6]. Indeed, *N*-phenylpyridinium salts have also been attracting interest in recent years [7–9]. With these dialkoxyphenylpyridine materials to hand and given the extensive previous investigations of related alkoxystilbazoles, it was then of interest to prepare some complexes of silver(I) to understand how the difference in ligand structure would influence the mesomorphism.

1.1. Synthesis

The ligands were prepared in a Suzuki-Miyaura coupling between 4-bromopyridine and the pinacol ester of 3,4-dialkoxyphenylboronic acid as described previously (Fig. 2) [6]. Complexes of silver(I) dodecyl sulfate (**1-*n***) were obtained by stirring the ligand with an excess of silver dodecyl sulfate overnight in dichloromethane at room temperature, protected from light. The reaction mixture was then filtered through celite and the filtrate evaporated to dryness; the residue was crystallised from hot acetone and washed with diethyl ether to afford the target complexes. Yields typically varied from 50 to 65% depending on the terminal chain length. Complexes with silver triflate (**2-*n***) were obtained by reaction of the ligand with AgOTf in acetone at room temperature ($n \leq 12$) or 50 °C ($n > 12$ – needed for ligand solubility) while protected from the light. After four hours, the reaction mixture was cooled to –18 °C and the resulting precipitate isolated *via* filtration, washed with multiple portions of cold acetone and air dried. Yields typically varied from 50 to 80% depending on the terminal chain length. Analytical data are found in the Experimental Section and in Table 5.

2. Results

The liquid-crystalline properties of the complexes were studied by polarised optical microscopy complemented by differential scanning calorimetry and then the phases were characterised further by small-angle X-ray scattering.

* Corresponding author.
E-mail address: duncan.bruce@york.ac.uk (D.W. Bruce).

https://doi.org/10.1016/j.molliq.2022.119707
0167-7322/

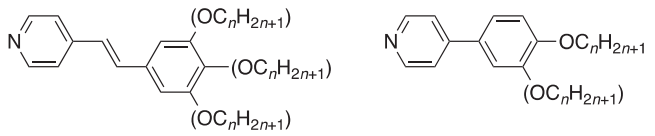

Fig. 1. Alkoxystilbazoles (left) and alkoxyphenpyridines (right).

2.1. Dodecyl sulfate salts – 1-n

The transition temperatures are found in Table 1 and are plotted as a phase diagram in Fig. 9a. The data show that the phase behaviour is dominated by the formation of a columnar phase for $6 \leq n \leq 14$, with two homologues (n = 4 and 6) also showing a cubic phase. Melting points are generally in the range 75–80 °C, while the clearing point rises from 99 °C for n = 4 to > 160 °C for n = 8 and 10, so that the mesophase range is 98 °C where n = 8.

Thus, on cooling from the isotropic liquid, the optical texture of the Col_h phase formed by compound **1–6** grows in from the isotropic liquid as large pseudo-focal-conic defects after which the cubic phase grows in slowly and supercooled as sharp edges at 67 °C as shown in Fig. 3a. Higher homologues displayed only an enantiotropic Col_h mesophase with pseudo focal-conic optical textures seen on cooling from the isotropic liquid. These homologues also formed glasses on cooling to room temperature, crystallising only slowly and sometimes over the course of several days.

Assignment of the columnar mesophase as hexagonal was confirmed by small-angle X-ray scattering (SAXS), where all derivatives with the exception of compound **1–6** displayed clear d_{10}, d_{11} and d_{20} reflections with relative spacings of $1 : 1/\sqrt{3} : 1/\sqrt{4}$. Complete diffraction data are presented in Table 2 and the SAXS data for **1–8** are plotted in Fig. 4. The lack of a d_{11} reflection for **1–6** implies less well-developed two-dimensional order, which may in turn reflect the presence of the underlying cubic phase. The hexagonal nature of the phase was, however, confirmed by a contact preparation with **1–8** in which the two were found to be co-miscible (Fig. 3b). The SAXS patterns also showed the presence of a broad and weak, mid-angle reflection at $2\theta \approx 8°$ (*ca* 10.5 Å) which it is postulated arises from longer-range metal–metal correlations which are often seen in the SAXS patterns of liquid crystals containing heavy transition elements (see for example references [10;11]).

As far as the cubic phase of **1–4** and **1–6** are concerned, we give only the strong reflection as the quality of the data at wider angles is much less good. As such, indexation is not possible and so estimation of a lattice parameter cannot be undertaken meaningfully. For example, the simplest possibility is that the strong reflection is the (1 0 0) of a simple cubic lattice. However, contrast this with our observations of related stilbazole complexes [12] where the first reflection was the (2 1 1) of a body-centred lattice, which would give a lattice parameter 2.5x greater. As such, we prefer to let the data stand without further speculation. This approach applies equally to the data for the cubic phase of complexes ***2-n***.

While the data in Table 2 show a steady increase in the columnar a parameter with increasing terminal chain length, its value is appreciably less than the calculated molecular length of the complexes (82% of the calculated length for **1–8** falling to 73% by **1–12** – Fig. 5). While some of this will be accounted for by chain folding and/or interdigitation, it is also likely that the complexes do not sit with their long axes perpendicular to the column direction in common with the accepted model for packing in the columnar phases of polycatenar mesogens [13].

2.2. Thermal behaviour of the triflate salts 2-n

The thermal data for these complexes are reported in Table 3, while the phase diagram is shown as Fig. 10a. The phase behaviour shows that the first two homologues studies (n = 4 and 6) were not mesomorphic and that as the chain length increased from 4 to 10, the melting point decreased quite steeply from 140 °C (**2–4**) to 83 °C (**2–10**). The first mesomorphic homologue is **2–8**, which melts at 102 °C to give a cubic phase as evidenced by the formation of a viscous and optically isotropic phase, which is seen also for **2–10**, **2–12** and **2–14**, the last of these also showing a columnar phase (Fig. 6 shows the cubic phase growing into the columnar phase for **2–14**). Complex **2–18** showed only the columnar phase. Interestingly, the stability of the cubic phase was relatively invariant with terminal chain length, while on its formation, the stability of the columnar phase increased steeply with terminal chain length.

In order to determine the symmetry of the columnar phase, SAXS data were recorded (Table 4) and the presence of a (10) and (11) reflection confirmed a hexagonal phase. In addition, a contact preparation was carried out between complexes **2–14** and **1–12**, which were found to be continuously miscible. For the

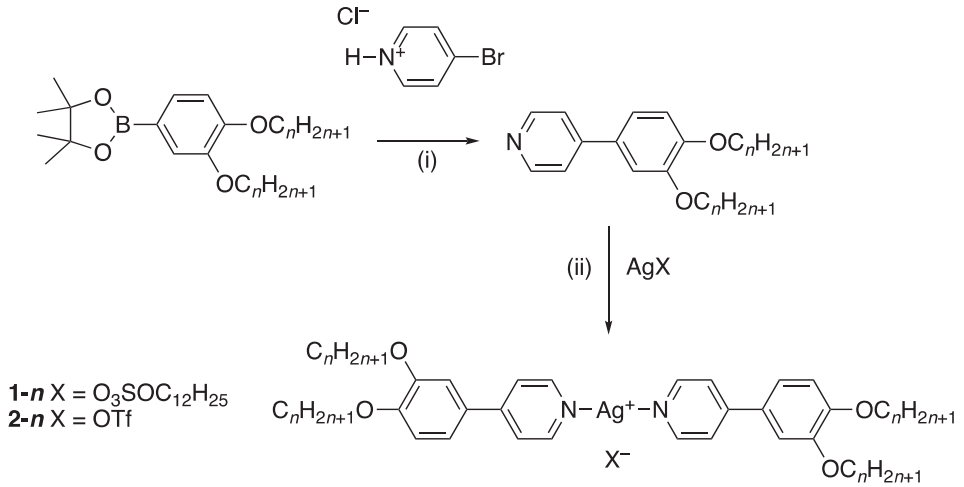

Fig. 2. Preparation of the 3,4-dialkoxyphenylpyridines and their complexes with silver(I) dodecylsulfate (**1** X = $O_3SOC_{12}H_{25}$ ({DOS}) and silver(I) triflate (**2** X = OTf). Conditions: (i) $[Pd_3(OAc)_6]$/SPhos/THF/H_2O/Na_2CO_3; (ii) X = OTf: acetone r.t. or 50 °C (see text); X = DOS: CH_2Cl_2 r.t.

Table 1
Transition temperatures from DSC for complexes **1-*n***.

n	Transition	*T*/°C	Δ*H*/kJ mol^{-1}
4	Crys - Cub	86	6.9
	Cub-Iso	99	0.7
6	Crys-Crys'	40	2.6
	Crys'-Crys''	61	7.5
	Crys'' - Cub	77	11.8
	Cub-Col$_h$	86	1.7
	Col-Iso	141	1.5
8	Crys-Col$_h$	68	38.1
	Col$_h$-Iso	166	2.5
10	Crys-Col$_h$	80	22.6
	Col$_h$-Iso	167	1.9
12	Crys-Crys'	49	14.7
	Crys'-Crys''	63	11.3
	Crys''-Col$_h$	74	7.9
	Col$_h$-Iso	154	1.0
14	Crys-Col$_h$	83	54.6
	Col$_h$-Iso	154	2.7

cubic phases, SAXS showed only a small number of low-angle reflections, which were, unfortunately, insufficient to identify the symmetry of the phase.

On cooling compounds **2–8, 2–10** and **2–12** from the cubic phase, crystallisation occurred slowly when held at or close to room temperature, with the exact temperature at which crystallisation occurred being dependent on the cooling rate. DSC was able to detect this crystallisation process, which often occurred as cold crystallisation on subsequent (re)heating cycles due to the slow kinetics of crystallisation from cubic phases.

In addition, cooling compound **2–6** from the isotropic liquid sometimes resulted in the formation of a monotropic mesophase that existed only for a short period of time (perhaps seconds), with the temperature at which it formed being very dependent on the cooling rate. This metastable phase was mostly homeotropic in nature, but some regions of a fan-like texture can be seen around the edges of the sample (Fig. 7). These observations are consistent

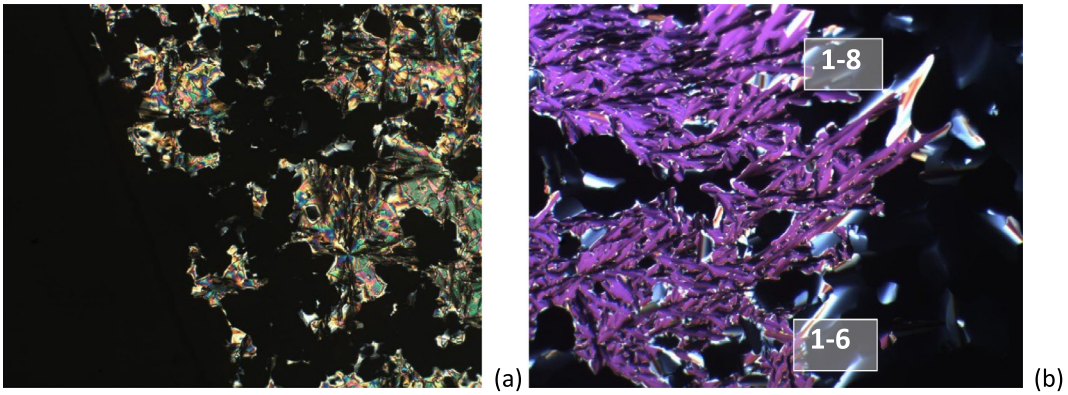

Fig. 3. Photomicrograph of: (a) the cubic phase growing in from the Col$_h$ phase on cooling compound **1–6** from the isotropic liquid at 59 °C and (b) contact preparation between **1** and **6** and **1–8** at 125 °C to show the hexagonal nature of the columnar phase in the former complex.

Table 2
Observed and calculated *d*-spacings from SAXS of the dodecyl sulfate salts (**1-*n***) the calculated molecular length of each cation assumes chains are in their all *trans* conformation.

n	*Phase*	*d*obs/Å	*d*calc/Å	*hk*	*Parameter*/Å	Calculated molecular length/Å
4	Cub	25.6				30.8
		4.7		halo		
6	Cub	27.7				35.9
		4.7		halo		
	Col$_h$	26.5		10	*a* = 30.6	
		15.4	15.3	11		
		13.3	13.3	20		
		10.0	10.0	21		
		4.5		halo		
8	Col$_h$	28.9		10	*a* = 33.4	41.0
		16.9	16.7	11		
		14.4	14.5	20		
		4.5		halo		
10	Col$_h$	30.9		10	*a* = 35.7	46.0
		17.9	17.9	11		
		15.4	15.5	20		
		4.5		halo		
12	Col$_h$	32.4		10	*a* = 37.4	51.1
		18.8	18.7	11		
		16.2	16.2	20		
		4.5		halo		
14	Col$_h$	34.2		10	*a* = 39.5	56.1
		19.8	19.8	11		
		17.0	17.1	20		
		4.5		halo		

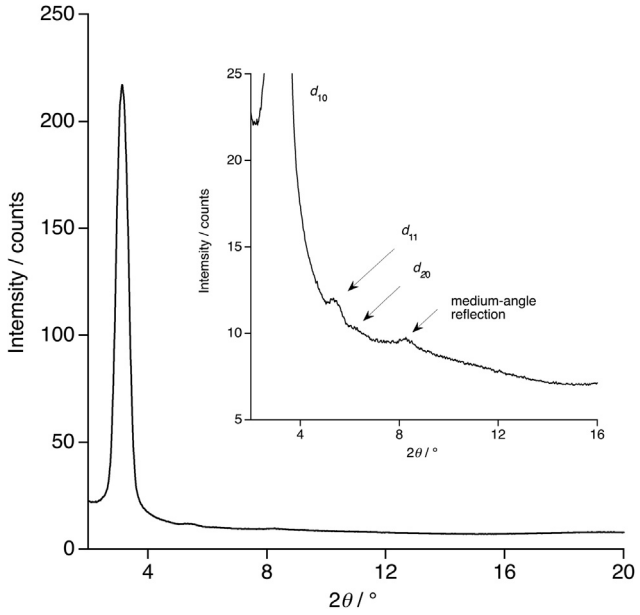

Fig. 4. Diffraction pattern for **1**–**8** at 83 °C in the Col_h phase; inset shows the d_{11}, d_{20} reflections and the broad, medium-angle reflection.

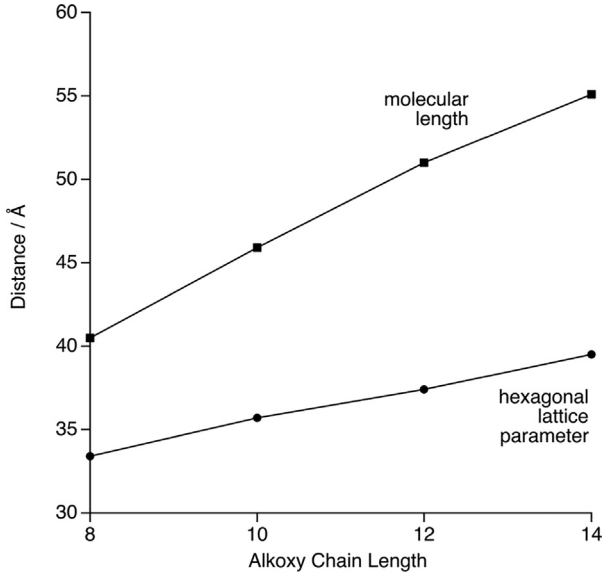

Fig. 5. Hexagonal lattice parameter (a) and calculated molecular length *vs* chain length for the series **1**-*n*.

with a metastable columnar phase, but this could not be reproduced by DSC neither SAXS measurements.

3. Discussion

There are three interesting comparisons to be made in relation to the mesomorphism of these new complexes – first to one another (Fig. 9a and 10a), then to the analogous stilbazole complexes (**3-*n*** and **4-*n*** – Fig. 8; phase diagrams in Fig. 9b and 10b) [14–15] and then finally to the related *N*-phenylpyridinium salts (**5-*n*** and **6-*n*** – Fig. 8; phase diagrams in Fig. 9c and 10c) [5,6].

Thus, in comparing **1-*n*** and **2-*n***, an early observation is that while both show cubic and a Col_h phases, the former is present for more chain lengths than the latter in the triflate salts. This is

Table 3
Thermal data of the triflate salts, **2-*n***, from DSC.

n	Transition	*T*/°C	Δ*H*/kJ mol^{-1}
4	Crys-Iso	140	65.3
6	Crys-Iso	122	25.6
8	Crys-Crys'	65	14.8
	Crys'-Cub	102	9.9
	Cub-Iso	112	1.9
10	Crys-Cub	83	27.2
	Cub-Iso	117	1.4
12	Crys-Crys'	85	34.4
	Crys'-Cub	96	73.3
	Cub-Iso	116	3.2
14	Crys-Cub	102	27.8
	Cub-Col_h	111	0.8
	Col_h-Iso	129	0.3
18	Crys-Col_h	114	152
	Col_h-Iso	153	1.9

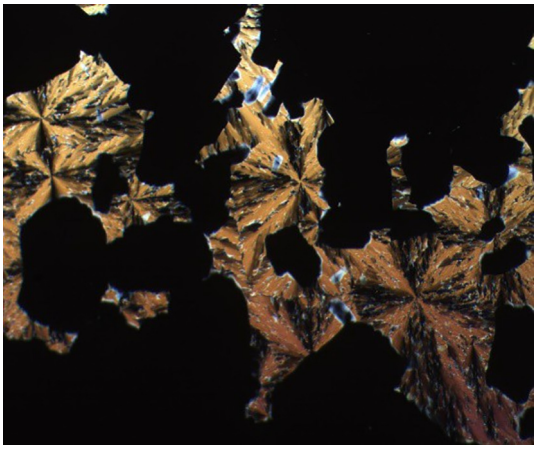

Fig. 6. Optical texture showing the cubic phase growing in from the Col_h phase of **2**–**14** at 102 °C on cooling.

unsurprising and relates first of all to arguments concerning surface curvature and its role in promoting the Cub-Col_h transition [16–17] and then to the observation that the dodecyl sulfate anion contributes to that curvature owing to its length [18], whereas the triflate anion does not. Next it is obvious that the stability of the mesophase observed depends very strongly on its identity. Thus, for the triflate salts, the cubic phase is stable to 110–120 °C, while for the two dodecyl sulfate salts that show a cubic phase, the clearing temperature are 99 and 86 °C. However, as soon as the columnar phase appears then the mesophase stability increases rapidly, reaching 167 °C for **1**–**10** and 153 °C for **2**–**18**. We have noted previously the significantly enhanced stability of columnar phases in such ionic systems [5,6].

Now in comparing the phenylpyridine and stilbazole complexes with a dodecyl sulfate anion (Fig. 7), it is apparent that, to a first approximation, the melting and clearing points are rather similar. Further, the clearing points increase very significantly when a Col_h phase is introduced. However, the major different is that while the cubic phase is seen only for the shortest homologue with the phenylpyridine complexes (**1**–**4**), in the stilbazole complexes it persists to the decyloxy homologue **3**–**10**. The major point of difference between the two series of materials is the length of the rigid core, which is *ca* 4.8 Å longer (≈2.4 Å/stilbazole) in the case of the stilbazole. Thus, once more, we invoke the observation that in silver stilbazole complexes, the dodecyl sulfate anion extends beyond the rigid core, contributes to surface curvature and so promotes the formation of phases where that curvature is higher (*e.g.* cubic

Table 4
Observed and calculated *d*-spacings from SAXS of the triflate salts (**2-*n***).

n	*Phase*	*d*obs/Å	*d*calc/Å	*hk*	*Parameter*/Å	Calculated molecular length/Å
8	Cub	29.9				41.0
		4.8		halo		
10	Cub	32.1				46.0
		4.8		halo		
12	Cub	34.6				51.1
		4.8		halo		
14	Cub	37.4				56.1
		4.8		halo		
	Col_h	34.2		10	a = 39.5	
		19.8	19.8	11		
		4.8		halo		
18	Col_h	36.0		10	a = 41.6	66.2
		20.8	20.8	11		
		18.4	18.0	20		
		4.8		halo		

Table 5
Analytical data for the new complexes.

		Found (calculated)		
n	Yield/%	%C	%H	%N
1–4	47	61.5 (61.8)	8.1 (7.8)	2.8 (2.9)
1–6	59	64.2 (64.3)	8.6 (8.5)	2.2 (2.6)
1–8	54	65.9 (66.3)	9.1 (9.0)	2.2 (2.3)
1–10	57	67.4 (67.9)	10.1 (9.5)	2.1 (2.1)
1–12	43	65.2 (65.4)	8.9 (8.8)	2.1 (2.2)
1–14	65	66.9 (67.0)	9.4 (9.3)	2.0 (2.0)
2–4	48	54.7 (54.7)	6.0 (5.9)	3.1 (3.3)
2–6	63	58.0 (58.3)	6.8 (6.9)	2.6 (2.9)
2–8	47	61.1 (61.2)	7.5 (7.7)	2.3 (2.6)
2–10	57	63.3 (63.5)	8.6 (8.3)	2.2 (2.4)
2–12	81	65.2 (65.4)	8.9 (8.8)	2.1 (2.2)
2–14	71	66.9 (67.0)	9.4 (9.3)	2.0 (2.0)
2–18	62	69.6 (69.5)	10.0 (10.0)	1.7 (1.7)

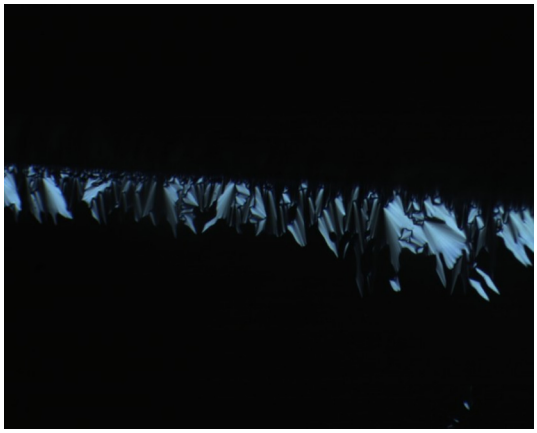

Fig. 7. Optical texture of the metastable columnar phase formed by the hexyloxy homologue, **2**–**6**.

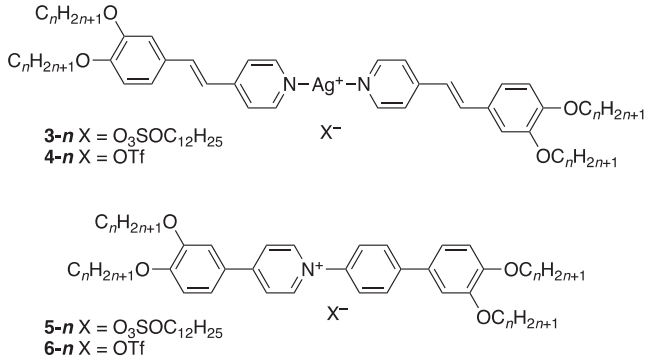

Fig. 8. Structures of the silver stilbazole complexes (**3-*n*** and **4-*n***) and *N*-phenylpyridinium salts (**3-*n*** and **4-*n***) for comparison.

vs lamellar or columnar *vs* cubic). The extension beyond the core is then clearly greater for the shorter phenylpyridine core which then explains the appearance of the Col_h phase at shorter chain lengths.

In then making the same comparison with the triflate salts (**2-*n*** and **4-*n***), what is immediately noticeable is that while the cubic phase persists to the same chain length in both series, the phase is some 40 °C more stable in the stilbazole complexes. It is difficult to be absolutely definitive in identifying the reason for this, but it is postulated that it is related to the overall shape as shown in Fig. 10. Thus, the rather linear nature of the phenylpyridine complexes (**4-*n***) means that the triflate counter-anion represents a greater perturbation to the anisotropy of the cation than in the stilbazole complexes (**2-*n***) because of the more angular nature of the latter consequent on the presence of the vinylic group (Fig. 11). It is well known from the liquid crystal chemistry of lateral fluorination that exchanging H for F can lead to a very significant destabilisation of mesophases [19–21] and it is proposed that the same generic effect of broadening is responsible here. Both series show a steeply declining melting point from n = 4 to n = 10 and the stability of the columnar phases continues to rise at the longest chain lengths.

It then remains to compare these new silver complexes with the related *N*-phenylpyridinium salts **5-*n*** and **6-*n*** [5–6]. The structural differences are the nature of the core of the cations, which is unsymmetric in the organic salts with the charge localised on the

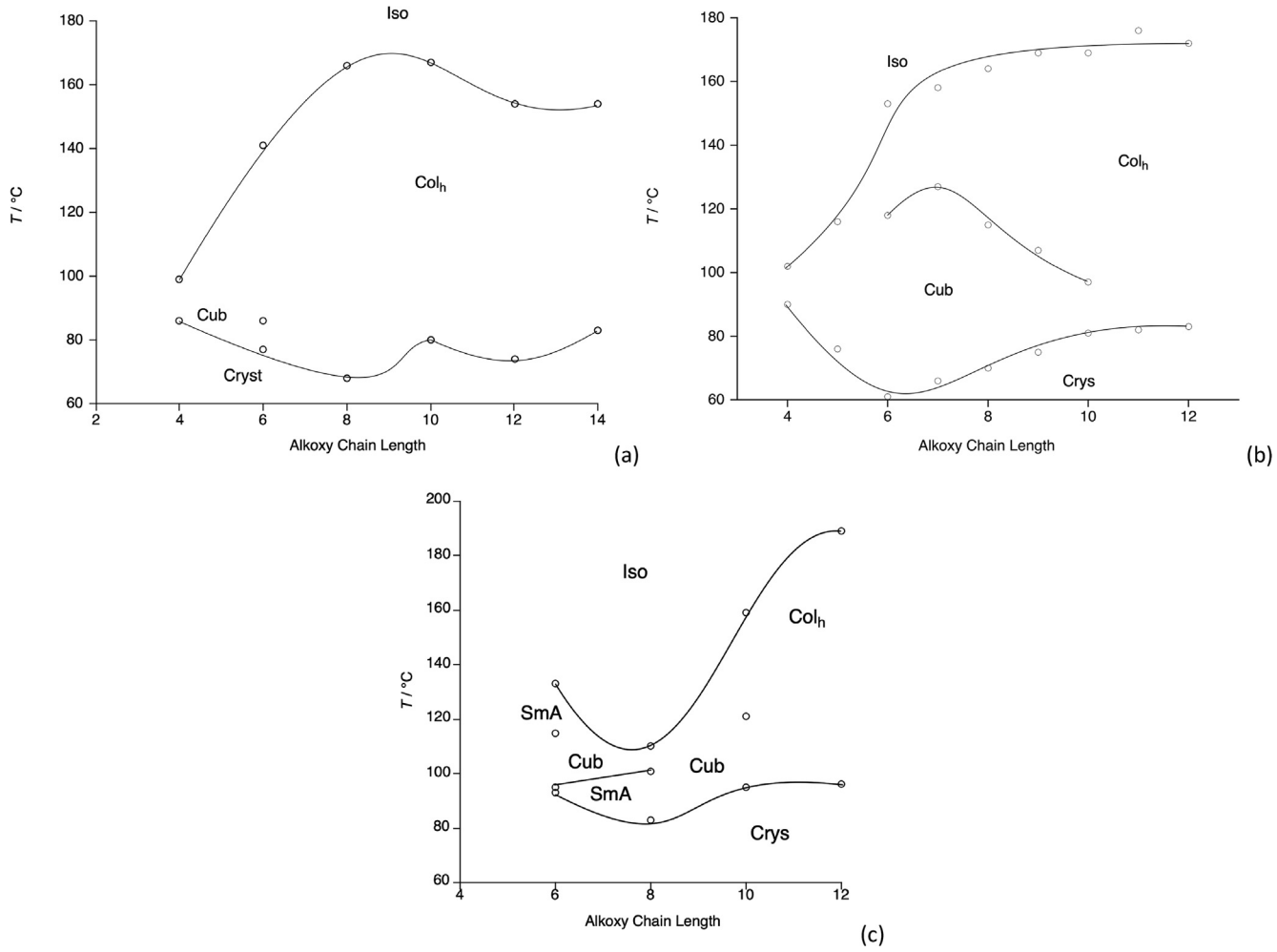

Fig. 9. Comparison of phase diagrams of (a) the phenylpyridine complexes (**1-*n***) and (b) the stilbazole complexes of silver(I) dodecyl sulfate (**3-*n***) and (c) the analogous *N*-phenylpyridinium dodecyl sulfate salts (**5-*n***). Diagrams (b) and (c) are replotted from published data.

pyridinium nitrogen, whereas the silver salts are symmetric with the anion able to approach closely as evidenced through various X-ray single crystal structures [22–24]. Indeed, no conductivity could be measured for the silver dodecyl sulfate salts [12] so that while there is clearly a build-up of electrostatic charge around the silver, they behave like covalent materials and their mesomorphism has been so interpreted. However, the charge in the *N*-phenylpyridinum salts is an additional factor and so if their dodecyl sulfate salts are considered, then a SmA phase is seen at shorter chain lengths along with a cubic phase, with a columnar phase appearing at **5**–**10**, again accompanied by a strong increase in clearing point (Fig. 8c). The formation of the SmA phase has been interpreted as reflecting both the electrostatic attraction between the oppositely charged ions and the fact that effective volume of the ionic core is increased by the counter-anion reducing surface curvature and allowing a lamellar phase to be seen [5–6]. This is seen more clearly in the triflate salts (**6-*n***) where there is only a SmA phase to **6**–**13**, with **6**–**14** showing a Col$_h$ phase with a huge increase in clearing point (Fig. 9c). No cubic phase is observed.

Thus, for the *N*-phenylpyridinium salts, their ionic nature is a very strongly defining feature of their behaviour that exerts control over the phases seen at shorter chain lengths. That said, all six series of materials show some or all of the phase progression found in tetracatenar mesogens as chain length increases, from lamellar to cubic to columnar phases. This is a delicate function of electrostatic factors and of the relative volumes and lengths of core and chains, but with the curious observation of strong phase stabilisation once a columnar phase is formed, which has been discussed previously [5,6].

4. Conclusion

The new silver complexes of 3,4-dialkoxystilbazoles with either dodecyl sulfate or triflate counteranions behave as fairly typical tetracatenar mesogens inasmuch as their mesomorphism is determined by interfacial curvature. In these complexes, this is driven by the tensioning of the terminal chain length, the volume of the rigid core including the anion and, in the case of the DOS salts, the extension of the anion chain beyond that core. In this regard, the comparison with analogous silver stilbazole complexes is helpful.

That the DOS anion chain extended beyond the rigid core to contribute to terminal chain volume is very well illustrated in comparing phenylpyridine and stilbazole complexes as in the former, with the shorter core, the Col$_h$ phase (promoted by greater interfacial curvature) appears at shorter terminal chain lengths. However, in the OTf salts where this is not a factor, then the differences between the two series in relation to phase appearance as a function of chain length are minimal. That said, the overall shape of the complexes does have an influence so that the greater linearity of the phenylpyridine complexes suffers greater distortion by the tri-

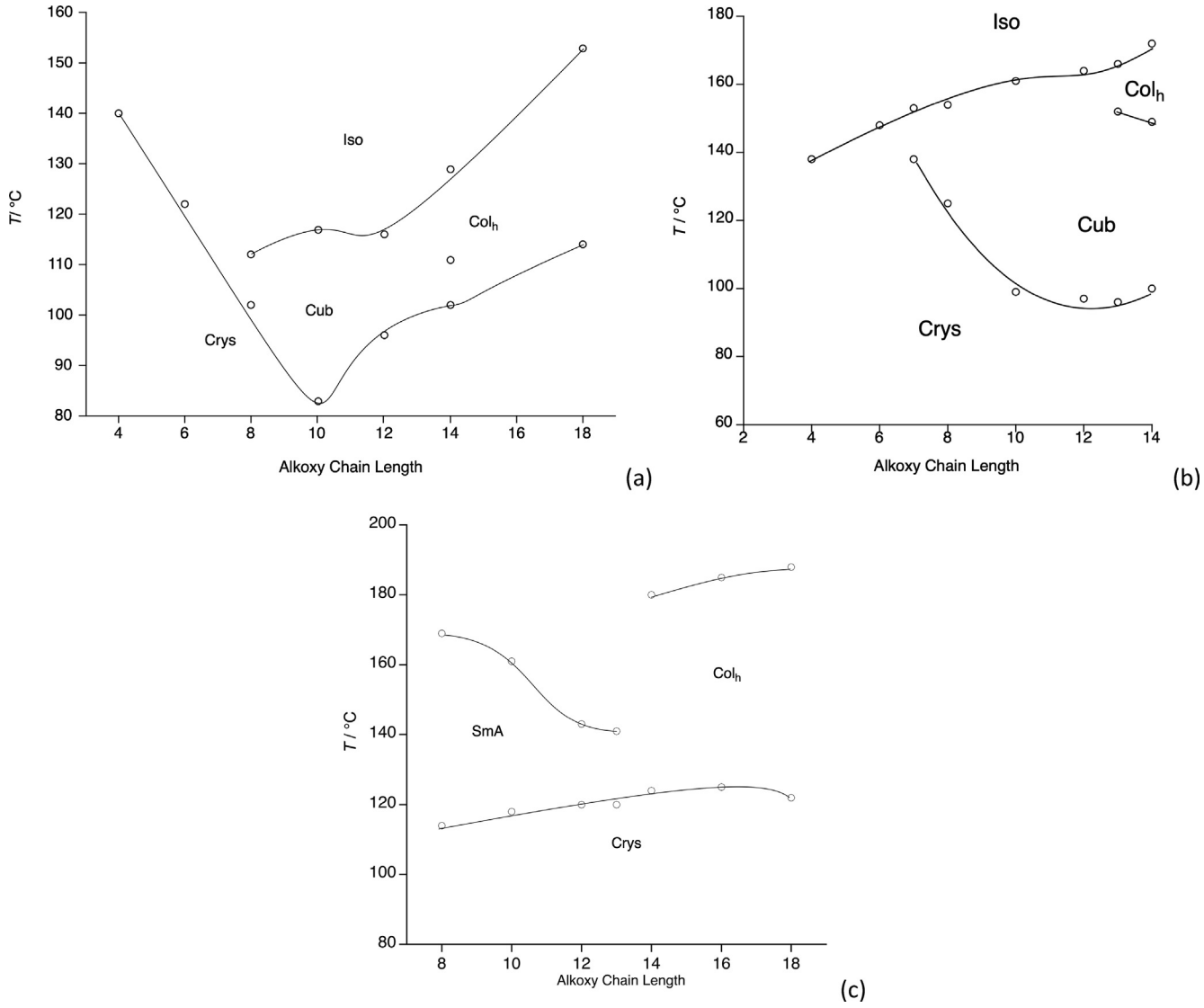

Fig. 10. Comparison of phase diagrams of (a) the phenylpyridine complexes (**2-*n***) and (b) the stilbazole complexes of silver(I) trifate (**4-*n***) and (c) the analogous *N*-phenylpyridinium triflate salts (**6-*n***). Diagrams (b) and (c) are replotted from published data.

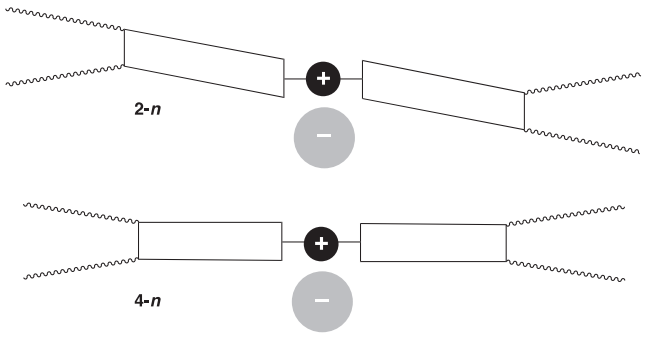

Fig. 11. Schematic representation of the overall shapes of complexes **2-*n*** and **4-*n***.

flate anion, reducing the anisotropy and therefore destabilising the crystal phase when compared to the stilbazole analogues.

What is known of these silver complexes is that the anions associate rather closely with the silver cations giving what is in effect a tight-bound ion pair and so while formally they are ionic, they tend to behave more as neutral compounds with a very polar core [25]. However, comparing the new silver complexes with the organic *N*-phenylpyridinium analogues reveals greater differences inasmuch as the *N*-phenylpyridinium salts will exist as ion-separated materials, which drives the appearance of a SmA phase at shorter chain lengths before giving way to a cubic and/or a Col$_h$ phase as predicted for a tetracatenar mesogen. Furthermore, for the triflate salts where the destabilising effect of the long-chain DOS anion is absent, the greater electrostatic component in the system is reflected in appreciably higher melting points.

Thus, while the new compounds and all of those with which they are compared follow the general and expected behaviour for tetracatenar mesogens, the detail is a subtle function of competing factors. The fact that these factors can be convincingly rationalised speaks strongly to the body of understanding developed through diverse studies over many years and makes a powerful case for the continuation of systematic work in the study of liquid crystals.

5. Experimental

^{1}H and ^{19}F NMR spectra were recorded on a Jeol ECS400 spectrometer equipped with a sample changer operating at 400 MHz

(^{1}H) or 376 MHz (^{19}F). Elemental analyses were performed by Dr Graeme McAllister at the University of York using an Exeter Analytical Inc CE 440 Elemental Analyzer and a Sartorius SE2 analytical balance.

Polarising optical microscopy was carried out using an Olympus BX50 polarising microscope equipped with a Linkam scientific LTS350 heating stage, Linkam LNP2 cooling pump, and Linkam TMS92 controller, differential scanning calorimetry was performed on a Mettler DSC822^e using Mettler STAR-E software, which was calibrated before use against indium and zinc standards under an atmosphere of dry nitrogen. Small-angle X-ray scattering was performed using a Bruker D8 Discover equipped with a bespoke temperature-controlled, bored graphite rod furnace, custom built at the University of York. The radiation used was copper K_α (λ = 0.154056 nm) from a 1 μS microfocus source. Diffraction patterns were recorded on a 2048 × 2048 pixel Bruker VANTEC 500 area detector set at a distance of 121 mm from the sample. Samples were filled into 0.9 mm capillary tubes.

Ligands were prepared as described previously [5]. Each family of silver complexes was prepared in the same way and a single example is given for each. Yields and CHN data for all of the new complexes are collected in Table 4.

5.1. Synthesis of the 3,4-dialkoxyphenylpyridine complexes of silver(I) dodecyl sulfate 1-n

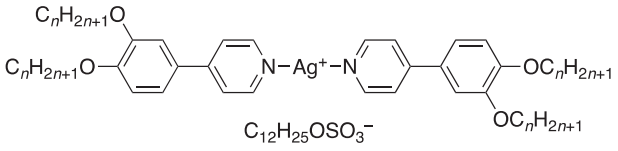

3,4-Didodecyloxyphenylpyridine (0.30 g, 0.57 mmol) was taken into dichloromethane (7 ml) and added dropwise to a stirred suspension of silver(I) dodecyl sulfate (0.12 g, 0.32 mmol) in dichloromethane (7 ml) in a vessel protected from light. The reaction mixture was stirred at room temperature overnight before filtration through a plug of celite followed by evaporation of the filtrate. The brown residue was then crystallised from hot acetone and the solid washed repeatedly with diethyl ether. The resulting solid was then taken into dichloromethane and filtered once more through a plug of celite to remove any insoluble by-products; the filtrate was the evaporated under reduced pressure to leave a white solid (43%): ^{1}H NMR (400 MHz, $CDCl_3$) δ = 8.74 (4H, AA′XX′, J = 6.5 Hz), 7.52 (4H, AA′XX′, J = 6.5 Hz), 7.14 (2H, dd, J = 8.5, 2.0 Hz), 7.10 (2H, d, J = 2.0 Hz), 6.90 (2H, d, J = 8.5 Hz), 4.11 (2H, t, J = 7.0 Hz), 4.02 (4H, t, J = 7.0 Hz), 4.02 (4H, t, J = 7.0 Hz), 1.84 (8H, m), 1.59 (2H, m), 1.47 (8H, m), 1.26 (82H, m), 0.85 (15H, m). ESI: found 1156.7916 [M + 1$^+$], 265.1485 [M$^-$].

5.2. Preparation of the tetracatenar 3,4-dialkoxyphenylpyridine silver (I) triflates 2-n

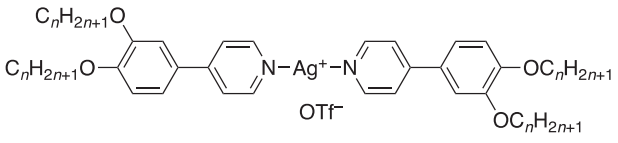

3,4-Didodecyloxyphenylpyridine (0.30 g, 0.57 mmol) was taken into acetone (20 ml) and the vessel protected from light. Silver triflate (0.08 g, 0.32 mmol) was then added and the reaction mixture stirred at 50 °C for 4 h, after which time it was placed in the freezer and the solid isolated *via* filtration. The product was then recrystallised from hot acetone and washed three times with diethyl ether. The resulting solid was then taken into dichloromethane and filtered through a plug of celite to remove any insoluble by-products; the solvent was then evaporated under reduced pressure to furnish a colourless powder (51%): ^{1}H NMR (400 MHz, $CDCl_3$) δ = 8.71 (4H, AA′XX′, J = 6.5 Hz), 7.56 (4H, AA′XX′, J = 6.5 Hz), 7.13 (2H, dd, J = 8.5, 2.0 Hz), 7.10 (2H, d, J = 2.0 Hz), 6.90 (2H, d, J = 8.5 Hz), 4.04 (4H, t, J = 7.0 Hz), 4.03 (4H, t, J = 7.0 Hz), 1.86 (8H, m), 1.50 (8H, m), 1.31 (64H, m), 0.89 (6H, t, J = 6.5 Hz), 0.89 (6H, t, J = 6.5 Hz). ^{19}F NMR (376 MHz, $CDCl_3$) δ_F = 77.68, (s). ESI: found 1156.7916 [M + 1$^+$], 148.9525 [M$^-$].

Declaration of Competing Interest

The authors declare that they have no known competing financial interests or personal relationships that could have appeared to influence the work reported in this paper.

Acknowledgements

The University of York is thanked for the provision of a studentship to JDH.

References

[1] D.W. Bruce, Acc. Chem. Res. 33 (2000) 831–840.
[2] D.W. Bruce, Adv. Inorg. Chem., 2001, **52**, Chpt 3, pp. 151-204.
[3] See e.g. D.W. Bruce in: Supramolecular Chemistry: From Molecules to Nanomaterials; J. W. Steed and P. A. Gale (eds), Wiley, Chichester, 2012, pp 3493-3514.
[4] L.J. McAllister, PhD Thesis, University of York, 2014.
[5] J.D. Herod, D.W. Bruce, Molecules 26 (2021) 2653.
[6] J.D. Herod, M.A. Bates, A.C. Whitwood, D.W. Bruce, Soft Matter 15 (2019) 4432–4436.
[7] R.-T. Wang, G.-H. Lee, C.K. Lai, J. Mater. Chem. C 6 (2018) 9430–9444.
[8] R.-T. Wang, G.-H. Lee, C.K. Lai, CrystEngComm 20 (2018) 2593–2607.
[9] R.-T. Wang, S.-J.-J. Tsai, G.-H. Lee, C.K. Lai, Dyes and Pigments 173 (2020) 107913.
[10] R.R. Parker, J.P. Sarju, A.C. Whitwood, J.A.G. Williams, J.M. Lynam, D.W. Bruce, Chem. Eur. J. 24 (2018) 19010–19023.
[11] A.M. Levelut, M. Ghedini, R. Bartolino, F.P. Nicoletta, F. Rusticelli, J. de Phys. 50 (1989) 113–119.
[12] D.W. Bruce, D.A. Dunmur, S.A. Hudson, E. Lalinde, P.M. Maitlis, M.P. McDonald, R. Orr, P. Styring, A.S. Cherodian, R.M. Richardson, J.L. Feijoo, G. Ungar, *Mol.* Cryst., Liq. Cryst., 1991, 206, 79-92.
[13] B. Donnio, B. Heinrich, H. Allouchi, J. Kain, S. Diele, D. Guillon, D.W. Bruce, J. Am. Chem. Soc. 126 (2004) 15258–15268.
[14] B. Donnio, D.W. Bruce, B. Heinrich, D. Guillon, H. Delacroix, T. Gulik-Krzywicki, Chem. Mater. 9 (1997) 2951–2961.
[15] B. Donnio, D.W. Bruce, New J. Chem. 23 (1999) 275–286.
[16] D. Guillon, B. Heinrich, A.C. Ribeiro, C. Cruz, H.T. Nguyen, Mol. Cryst. Liq. Cryst. 317 (1998) 51–64.
[17] M. Gharbia, A. Gharbi, H.T. Nguyen, J. Malthête, Curr. Opin. Coll. Interfac. Sci. 7 (2002) 312–325.
[18] D.W. Bruce, B. Donnio, S.A. Hudson, A.-M. Levelut, S. Megtert, D. Petermann, M. Veber, J. Phys. II France 5 (1995) 289–302.
[19] P. Kirsch, J. Fluorine Chem. 177 (2015) 29–36.
[20] M. Bremer, P. Kirsch, K. Klasen-Memmer, K. Tarumi, Angew. Chem., Int. Ed. 52 (2013) 8880–8896.
[21] M. Hird, Chem. Soc. Rev. 36 (2007) 2070–2095.
[22] H. Adams, N.A. Bailey, D.W. Bruce, S.C. Davis, D.A. Dunmur, S.A. Hudson, S.J. Thorpe, J. Mater. Chem. 2 (1992) 395–400.
[23] D.M. Huck, H.L. Nguyen, S.J. Coles, M.B. Hursthouse, D. Guillon, B. Donnio, D.W. Bruce, Polyhedron 25 (2006) 307–324.
[24] H.L. Nguyen, P.N. Horton, M.B. Hursthouse, D.W. Bruce, Liq. Cryst. 31 (2004) 1445–1456.
[25] A.I. Smirnova, D.W. Bruce, J. Mater. Chem. 16 (2006) 4299–4306.